Acta Pharmaceutica Sinica B 2026;16(6):3861−3875

Chinese Pharmaceutical Association
Institute of Materia Medica, Chinese Academy of Medical Sciences

Acta Pharmaceutica Sinica B

www.elsevier.com/locate/apsb
www.sciencedirect.com

ORIGINAL ARTICLE

Microthrombi targeted nano-micelle synchronizing endothelial gap opening and matrix decompression for augmenting drug perfusion within pancreatic cancer

Mengnan Yang[a,†], Yuqing Tong[a,†], Shaoping Yin[b,†], Hengchuan Zhang[a], Xiaowen Huang[a], Kai Yuan[c], Yanfei Hao[d], Jianping Zhou[a,*], Meirong Huo[a,*], Tingjie Yin[a,*]

[a]*Department of Pharmaceutics, China Pharmaceutical University, Nanjing 211198, China*
[b]*External Medication Development and Application, Nanjing University of Chinese Medicine, Nanjing 210023, China*
[c]*Department of General Surgery, The First Affiliated Hospital of Shandong First Medical University, Jinan 250014, China*
[d]*Cheeloo College of Medicine, Shandong University, Jinan 250012, China*

Received 12 August 2025; received in revised form 8 October 2025; accepted 23 October 2025

KEY WORDS

Pancreatic ductal adenocarcinoma;
Endothelial barrier;
Tumor matrix;
Interstitial fluid pressure;
Antiplatelets;
Pancreatic stellate cells;
Blood perfusion;
Micelle-based nanodrug

Abstract Local inhibition of the "patching" function of tumor-associated platelets against neutrophil infiltration-caused vascular breaches has been used as an "enhanced permeability and retention (EPR) amplification" strategy. Nevertheless, the vascular leakage-resulted elevation of interstitial fluid pressure (IFP) could impact tumoral perfusion and convection of nanodrugs. Especially for hypoperfused and desmoplastic pancreatic ductal adenocarcinoma (PDAC), solely relying on vascular destruction would predictably diminish tumoral drug perfusion. According to multi-thrombosis formation in PDAC, a microthrombi and matrix co-targeted dasatinib (DAS) nano-micelle (CPHD/DAS) synchronizing endothelial gap opening and matrix decompression was constructed for sustained augmentation of drug perfusion within PDAC. CPHD/DAS was composed of CREKA peptide-modified hyaluronic acid−deoxycholate conjugates co-assembled with DAS. *In vitro* and *in vivo* results demonstrated CPHD/DAS not only retarded tumor-associated platelet activation to enhance vascular permeability and expose subvascular matrix, but also inhibited pancreatic stellate cell activation to alleviate stroma

*Corresponding authors.
E-mail addresses: cpu_zhoujp@163.com (Jianping Zhou), huomeirongcpu@163.com (Meirong Huo), cookey_89ytj@163.com (Tingjie Yin).
†These authors made equal contributions to this work.
Peer review under the responsibility of Chinese Pharmaceutical Association and Institute of Materia Medica, Chinese Academy of Medical Sciences.

https://doi.org/10.1016/j.apsb.2025.12.037

barrier. Thus, the matrix decompression resisted IFP elevation caused by endothelial gap opening, facilitating sustained up-regulation of functional vessels. Based on superior tumor accumulation and penetration, CPHD/DAS exhibited favorable potency in Panc02 tumor model. This study provides a paradigm to improve the efficiency and application scope of "EPR amplification" strategy in antitumor therapy.

1. Introduction

Pancreatic ductal adenocarcinoma (PDAC) is characterized by dense extracellular matrix (ECM)[1,2]. ECM not only increases tumoral solid stress but also increases interstitial fluid pressure (IFP) *via* promoting water retention[3,4]. First, the elevated solid stress and IFP compress tumor blood vessels, causing vasculature deformation and a reduced pressure difference of tissue perfusion, ultimately leading to characteristic hypoperfusion[2,5−7]. Secondly, the vascular gap resulting from inflammatory cell (*e.g.*, neutrophil) infiltration can be physically sealed by local platelet activation-induced dynamic thrombi. The activated platelets also release soluble platelet factors to further mediate biochemical repair of endothelial junctions[8,9]. They collectively attenuate endothelial leakage. Thirdly, the elevated IFP hinders the convective extravasation of therapeutic drugs (especially nanodrugs) from blood vessels into tumor ECM[5,10,11]. Thus, the enhanced permeability and retention (EPR)-based tumoral drug accumulation is impeded by the "leakage obstacles" which refer to limited blood perfusion, reduced vascular leakage and increased IFP. Worse still, the dense matrix further restricts the effective penetration of accumulated drugs into the deep tumor site[12−14]. Briefly, the therapeutic efficiency of EPR-based nanodrugs against PDAC is severely constrained.

The efficacy of clinical chemotherapy for PDAC is relatively limited, and one key reason is the compromised drug infiltration imposed by the stromal microenvironment[1,15]. Consequently, current preclinical researches primarily focus on inactivating or inducing quiescence of pancreatic stellate cells (PSCs) to recover stromal homeostasis[16−19]. However, this approach is restricted by the presence of "leakage obstacles" which hinder the prerequisite accumulation of drugs within tumor[2,20]. Studies have focused on the physical and biochemical "patching" function of the activated platelets in neutrophil infiltration-caused vascular gaps. Specific depletion of tumor-associated platelets or local inhibition of platelet activation has been demonstrated to increase endothelial leakage[21,22]. The effectiveness of this strategy in augmenting drug delivery to tumor was validated in breast, cervical, colon, and bladder tumors[21−25]. Nevertheless, these studies have not comprehensively considered the potential consequences of increased vascular leakage on elevating IFP, which could impact the subsequent tumoral perfusion and the transvascular convection of nanoparticles. Especially for hypoperfused and desmoplastic tumors like PDAC, solely relying on this EPR amplification strategy would further diminish intratumoral drug perfusion[26].

PDAC demonstrates characteristic high expression of tissue factors. These tissue factors promote thrombi formation by converting fibrinogen to insoluble fibrin which subsequently solidifies around the activated platelets. Therefore, except for the formation of dynamic thrombi for endothelial repair, the endogenous incidence of pathologic microthrombi in PDAC is significantly higher compared to the other solid tumors[27,28]. Thus, according to the hypoperfusion and propensity for multi-thrombosis formation in PDAC, we developed a thrombus and matrix targeted dasatinib nano-micelle (CPHD/DAS) which synchronously inactivated local platelets for endothelial gap opening and PSCs for matrix decompression. As shown in Scheme 1, CPHD/DAS was composed of CREKA peptide-modified amphipathic hyaluronic acid−deoxycholate conjugates (CPHD) co-assembled with dasatinib (DAS) in aqueous phase. In our previous work, amphipathic hyaluronic acid−deoxycholate conjugates (PHD) were established as a well-recognized nanomaterial with controllable synthesis, a low critical micelle concentration (CMC), and hyaluronidase (HAase) responsiveness[29], achieving superior encapsulation efficiency and drug loading for DAS compared with reported formulations[30−33]. To further enhance tumor selectivity, PHD was conjugated with the CREKA peptide, which specifically targeted fibrin within microthrombi in the tumor vessel wall and extracellular matrix abundantly present in PDAC[34−36]. The resulting CPHD micelles thus integrated structural stability, high drug-loading capacity, tumor-associated fibrin targeting, and HAase-responsive drug release within the tumor microenvironment (TME). DAS was a multi-target tyrosine kinase inhibitor that disrupted the function of SRC kinases in platelets to suppress collagen and podoplanin-induced activation cascades[37−39]. Besides, SRC kinases belong to the downstream targets of platelet-derived growth factor receptor and transforming growth factor β (TGF-β) signaling. DAS could not only inhibit the over-activation of PSCs, but also decrease the proliferation and metastasis of tumor cells through blocking SRC kinases[40,41].

When intravenously administrated, CPHD/DAS specifically accumulated around microthrombi which were abundant in PDAC. The locally released DAS inactivated perivascular platelets, and thus disrupted their role in repairing endothelial gap. The sub-vascular matrix exposure and CREKA-mediated matrix targeting established positive feedback-based self-propelling. In the following, the accumulated DAS weakened matrix barrier and promoted drug infiltration by suppressing the activation of PSCs. Most importantly, the reduction in solid stress mediated by CPHD/DAS gradually counteracted the negative effects of increased IFP caused by the EPR amplification strategy, facilitating sustained up-regulation of the functional vessels during the treatment. Resultantly, a deep tumoral drug distribution and an enhanced overall therapeutic outcome would be achieved. Based on the comprehensive consideration of factors in TME affecting drug perfusion, our strategy provides a new paradigm to further improve the application efficiency and expand the application scope of the EPR amplification strategy in antitumor therapy. It also offers new insights into effective therapeutic strategies for PDAC.

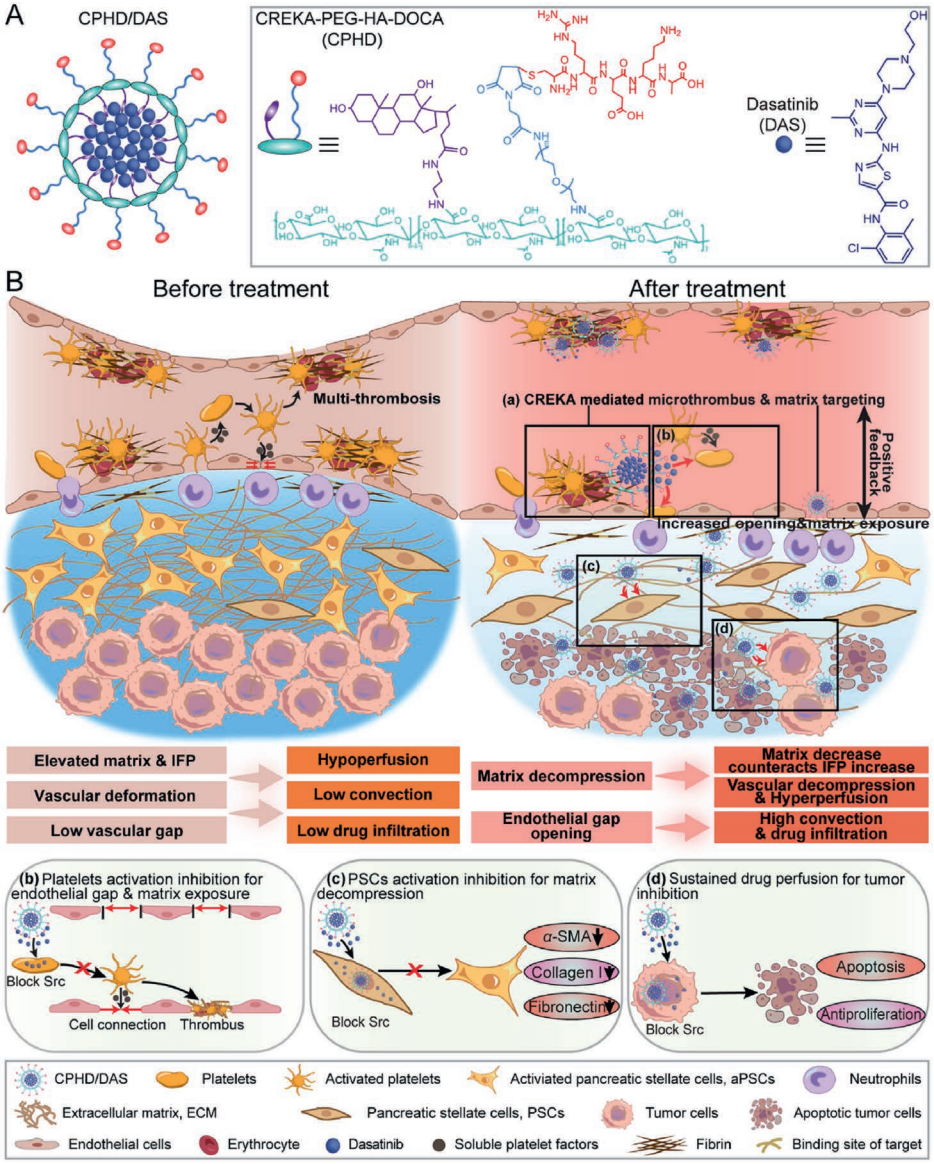

Scheme 1 Overview of CPHD/DAS design and function. (A) Schematic illustration of CPHD/DAS construction. (B) Schematic illustration of CPHD/DAS synchronizing endothelial gap opening and matrix decompression for augmenting drug perfusion within PDAC.

2. Materials and methods

2.1. Materials

Hyaluronic acid (HA = 10 kDa), deoxycholic acid (DOCA), pyrene, and Nile red were purchased from Macklin (Shanghai, China). Ethylenediamine and *N*,*N*′-dicyclohexylcarbodiimide were purchased from Nanjing Reagent (Nanjing, China). *N*-Hydroxysuccinimide (NHS) and 1-ethyl-3 (3-dimethylaminopropyl) carbodiimide (EDC) were purchased from Yien Chemical Technology Co., Ltd. (Shanghai, China). Maleimide-PEG3400-NH_2 (Mal-PEG3400-NH_2) was purchased from Ponsure Biological Technology Co., Ltd. (Shanghai, China). CREKA peptide was purchased from China Peptides Co., Ltd. (Shanghai, China). Tris-(2-carboxyethyl)-phosphine hydrochloride and DAS were purchased from Aladdin Biochemical Technology Co., Ltd. (Shanghai, China). 3,3′-Dioctadecyloxacarbocyanine perchlorate (DiO), 1,1′-dioctadecyl-3,3,3′,3′-tetramethylindocarbocya-nine perchlorate (DiI), thrombin, HAase, MTT, Annexin V-FITC/PI apoptosis detection kit, BCA protein assay kit and Hoechst 33342 were purchased from Beyotime Biotechnology Co., Ltd. (Shanghai, China). Rabbit polyclonal antibodies against phospho-SRC (*p*-SRC), α-SMA, fibronectin, collagen type I, GAPDH, horseradish peroxidase-conjugated goat anti-rabbit IgG and secondary Alexa Fluor 488-conjugated goat anti-rabbit IgG were purchased from Absin Bioscience Inc. (Shanghai, China). Near-infrared dye Cyanine7 (Cy7) was purchased from Fanbo Science Co., Ltd. (Beijing, China). D-luciferin potassium salt was purchased from MKbio Biotechnology Co., Ltd. (Shanghai, China).

2.2. Cells and animals

Rat PSCs line, LTC-14, obtained from American Type Culture Collection, was cultured in Iscove's modified Dulbecco's medium (Gibco, Thermo Fisher Scientific, Waltham, MA, USA) containing fetal bovine serum (FBS, 10%, *v*/*v*) (Thermo Fisher Scientific,

Waltham, MA, USA) at 37 °C with 5% CO_2 atmosphere. Mouse PDAC line, Panc02 and Panc02 transfected with the luciferase gene (Panc02-Luc), purchased from Zhong Qiao Xin Zhou Biotechnology (Shanghai, China), were cultured in Dulbecco's modified Eagle's medium (Gibco, Thermo Fisher Scientific, Waltham, MA, USA) supplemented with 10% FBS at 37 °C with 5% CO_2 atmosphere. All culture media were supplemented with 1% penicillin and streptomycin. Specifically, for activated PSCs, LTC-14 cells were treated with Iscove's modified Dulbecco's medium supplemented with 10 ng/mL of TGF-β (PeproTech, Cranbury, NJ, USA).

Female C57BL/6 mice (6 to 8-week age, 18−20 g) and male Sprague−Dawley (SD) rats (180−220 g) were purchased from Qinglongshan Animal Breeding Center (Nanjing, China). All animal experiments were approved by the Institutional Animal Care and Use Committee of China Pharmaceutical University (2021-09-017). To construct the orthotopic mouse PDAC model, 25 μL saline containing Panc02-Luc cells (1×10^6) was mixed with 25 μL Matrigel (Corning Inc., Corning, NY, USA) and orthotopically injected into the pancreatic tails of C57BL/6 mice.

2.3. Synthesis of CPHD conjugates and PHD conjugates

The synthesis scheme (Supporting Information Fig. S1) of CPHD conjugates and PHD conjugates was referred to the reported literature[29].

2.3.1. Synthesis of HA-DOCA amphiphilic conjugates

DOCA (1 g), *N*,*N*′-dicyclohexylcarbodiimide (0.63 g), and NHS (0.38 g) were dissolved in 15 mL of tetrahydrofuran and reacted for 12 h at room temperature under nitrogen. After that, the precipitate in the reaction solution was removed by filtration. *n*-Hexane was added to the filtrate, then the precipitate was placed in the vacuum dryer (DZF-6020, Changzhou Nuo Da Instrument Technology Co., Ltd., Changzhou, China) to obtain DOCA succinimidyl ester. Next, DOCA succinimidyl ester dissolved in 10 mL of *N*,*N*-dimethylformamide (DMF) was added into 15 mL of ethylenediamine. After being stirred for 12 h at room temperature, white precipitate was extracted from the reaction solution with distilled water addition, and amino-DOCA was obtained after vacuum drying.

HA (200 mg) was dissolved in 30 mL of formamide and then EDC (59 mg) and NHS (36 mg) were added. The mixture was stirred for 30 min to activate the carboxyl groups of HA. Amino-DOCA dissolved in DMF was dropped into the above activation reaction. The reaction was continued for 24 h at room temperature. The reaction mixture was poured into excess cold diethyl ether and the precipitate was extracted by filtration. After being redissolved with distilled water, the HA-DOCA conjugate was obtained by 48 h of dialysis (MWCO 7000 Da) and lyophilization.

2.3.2. Synthesis of PEGylated HA-DOCA amphiphilic conjugates (PEG-HA-DOCA, PHD)

HA-DOCA (50 mg) was dissolved in 10 mL of formamide and then EDC (400 mg) and NHS (180 mg) were added. The reaction solution was stirred for 30 min to activate the carboxyl groups of HA-DOCA. Then, Mal-PEG3400-NH_2 (42 mg) was added into the reaction solution, and the reaction was continued for 24 h at room temperature. The PHD amphiphilic conjugate was obtained by 48 h of dialysis (MWCO 14000 Da) and lyophilization.

2.3.3. Synthesis of CREKA modified HA-DOCA amphiphilic conjugates (CREKA-PEG-HA-DOCA, CPHD)

PHD (50 mg) was dissolved in 10 mL of formamide, and then CREKA peptide (8.3 mg) dissolved in 5 mmol/L tris-(2-carboxyethyl)-phosphine hydrochloride solution (pH 7.4) was added. The reaction was performed for 24 h in an ice bath under nitrogen protection. Then the mixture solution was dropped into 30 mL of distilled water. The CPHD amphiphilic conjugate was obtained by dialysis (MWCO 14,000 Da) for 48 h and lyophilization.

2.4. Characterization of CPHD conjugates and PHD conjugates

HA-DOCA, PHD and CPHD were weighed and mixed with an appropriate amount of KBr powder. After grinding and tablet pressing, the infrared spectrometer (TENSOR 27, Bruker, Billerica, MA, USA) was used for detection and FT-IR spectra were recorded. HA-DOCA, PHD and CPHD were weighed and dissolved in D_2O/CD_3OD ($v/v = 1:1$) mixed solution. Advance 500 nuclear magnetic resonance instrument (Bruker, Billerica, MA, USA) was used for detection and ^1H NMR spectra were recorded. The mass percentage of CREKA peptide (DS, *w*/*w*) in CPHD conjugates was determined by Perkin-Elmer 2400 elemental analyzer (PerkinElmer, Waltham, MA, USA) and calculated based on the introduction of new element S according to Eq. (1).

$$\text{DS of CREKA}\ (\%) = [(M_{\text{CREKA}} \times W_S) / M_S] \times 100 \quad (1)$$

Where M_{CREKA} and M_S is the relative molecular weight of CREKA and S, respectively, while W_S is the mass percentage of S element measured in elemental analysis. CPHD and PHD self-assembled micelles were prepared by the direct dissolution method. 15 mg of CPHD or PHD was dissolved in 2 mL of distilled water, then the solution was sonicated for 10 min at 100 W in an ice bath by ultrasonic probe (Beidi-II, Nanjing Beidi Experimental Instrument Co., Ltd., Nanjing, China) and filtered through 0.8 μm pore-sized microporous membrane to obtain CPHD and PHD micelles. The hydrodynamic diameter, size distribution and Zeta potential of the micelles were measured by dynamic light scattering (DLS) using Malvern Zetasizer Nano-ZS90 (Malvern Instruments, UK). The CMC of CPHD or PHD conjugates was monitored by the pyrene fluorescence probe method[42].

2.5. Preparation and characterization of drug-loaded nano-micelles

CPHD/DAS and PHD/DAS were prepared by the dialysis method referred to the reported literature[29]. Briefly, 15 mg of PHD or CPHD was dissolved in 2 mL of distilled water. 5 mg of DAS dissolved in 50 μL DMF was slowly added, and the mixture was vigorously agitated for 10 min. The resulting solution was sonicated for 10 min at 100 W in an ice bath with a probe-type ultrasonicator (Beidi-II, Nanjing Beidi Experimental Instrument Co., Ltd., Nanjing, China) and then dialyzed against distilled water for 12 h. After centrifugation and filtration (0.8 μm), the final preparation was obtained.

The hydrodynamic diameter, size distribution, and Zeta potential of CPHD/DAS or PHD/DAS were measured by DLS. The morphology of CPHD/DAS or PHD/DAS was characterized by transmission electron microscopy (HT7800, Hitachi, Tokyo, Japan) using a negative staining method. The content of DAS in nano-micelles was measured by an ultraviolet spectrophotometer

(Cary 60, Agilent Technologies, Santa Clara, CA, USA), while the ultraviolet detection wavelength was set at 323 nm. The entrapment efficiency (EE) and drug-loading (DL) were calculated according to Eqs. (2) and (3):

$$\text{EE}\,(\%) = (\text{weight of DAS in micelles} \,/\, \text{feeding weight of DAS}) \times 100 \quad (2)$$

$$\text{DL}\,(\%) = (\text{weight of DAS in micelles} \,/\, \text{weight of the micelles}) \times 100 \quad (3)$$

The *in vitro* stability of drug-loaded micelles was evaluated by DLS. PHD/DAS or CPHD/DAS was diluted with distilled water, 10% (*v*/*v*) FBS PBS buffer or Dulbecco's modified Eagle's medium, respectively. The samples were placed in a 37 °C, 100 rpm incubator (THZ-98C, Jintan Jingda Instrument Manufacturing Co., Ltd., Changzhou, China). Samples were taken out at the specific time intervals (0, 2, 4, 6, 10, 12 and 24 h) to examine size change.

An appropriate amount of DAS was added to PBS buffer (pH 7.4 or pH 5.0) and vortexed vigorously for 30 s at 5 min intervals. After 30 min, the concentration of DAS in the supernatant was determined by high-performance liquid chromatography (HPLC, Agilent 1100 system, Agilent Technologies, Santa Clara, CA, USA) equipped with an Agilent TC-C18 column (5 μm, 250 mm × 4.6 mm) referred to the reported literature[29]. The mobile phase was consisted of acetonitrile and NaH_2PO_4 buffer solution at pH 6.5 (40:60, *v*/*v*) and was run isocratically at a flow rate of 1.0 mL/min. The injection volume was 20 μL, and the detection wavelength was set at 323 nm. The release kinetics of DAS were evaluated *via* a dialysis method[29]. Briefly, 1 mL of CPHD/DAS or PHD/DAS solution containing 0.5 mg DAS was placed in a dialysis bag (MWCO = 7000 Da) and then immersed in 250 mL of PBS buffer solutions (pH 7.4 or pH 5.0) containing 0.3% (*w*/*v*) Tween 80. The experiment was performed in an incubator shaker at 37 °C at 100 rpm (THZ-98C, Jintan Jingda Instrument Manufacturing Co., Ltd., Changzhou, China). At predetermined time points (0, 1, 2, 3, 4, 6, 10, 16, 24, 36 and 48 h), 1 mL of release media was taken out and an equal volume of fresh medium was supplemented. The DAS concentration was measured by HPLC. HAase is abundant in PDAC microthrombus, interstitial microenvironment and lysosomes. To simulate DAS release from the nano-micelles during bio-transport, 1 mL of CPHD/DAS or PHD/DAS solution was immersed in the release media (pH 6.5 or pH 5.0) containing 0.5 mg/mL of HAase. The DAS concentration was determined as described above. Additionally, CPHD/DAS was immersed in pH 6.5 release media with activated platelets or resting platelets to characterize the release kinetics of DAS.

2.6. *In vivo stability and pharmacokinetic analysis*

DiO and DiI were used as a fluorescence resonance energy transfer (FRET) pair co-loaded with DAS to obtain the FRET PHD/DAS and FRET CPHD/DAS. The preparation was as described above, apart from the change of DAS addition to DiO and DiI addition. The SD rats were i.v. administered with FRET PHD/DAS or FRET CPHD/DAS. At predetermined time intervals, the blood samples were collected and centrifuged. The plasma supernatant was diluted with PBS. The fluorescence intensities of the samples at 501 and 565 nm were detected by a microplate reader (Thermo Fisher Scientific, Varioskan LUX) at an excitation wavelength of 484 nm. The FRET ratio was calculated according to Eq. (4):

$$\text{FRET ratio}\,(\%) = I_{565} \,/\, (I_{565} + I_{501}) \times 100 \quad (4)$$

where I_{501} and I_{565} were the emissions of DiO and DiI at 501 and 565 nm, respectively. Free DAS, PHD/DAS or CPHD/DAS was i.v. injected into the SD rats (at a dose of 5 mg/kg DAS). Blood samples were collected at predetermined time intervals. The samples were centrifuged and the supernatants were collected. The supernatants were mixed with acetonitrile and centrifuged. The DAS concentration in supernatants was then detected by HPLC.

2.7. *Hemolysis test*

Blood was taken from the orbit of rats and then treated with normal saline to obtain 2% blood cell suspension. Different concentrations of blank micelles (CPHD, PHD) and drug-loaded micelles (CPHD/DAS, PHD/DAS) were mixed with blood cell suspension. 5% glucose and distilled water were used as negative (A_0) and positive control ($A_{100\%}$), respectively. The above mixture solutions were incubated in a 37 °C water bath for 1 h and then centrifuged at 3000 rpm (Sorvall Legend Micro 21R, Thermo Fisher Scientific, Waltham, MA, USA) for 10 min. The absorbance of the supernatants was measured at 540 nm by a microplate reader. The hemolysis percentage of each group was calculated according to Eq. (5):

$$\text{Hemolysis}\,(\%) = \left(A_{\text{sample}} - A_0\right) \,/\, (A_{100\%} - A_0) \times 100 \quad (5)$$

2.8. *Platelet adhesion and aggregation test*

Thrombin is a key enzyme produced by vascular endothelial cells at the site of injury, which can activate platelets[43]. The collected platelets were labeled with DiI and activated with thrombin in confocal dishes, followed by being treated with 12 μL of free DAS, PHD/DAS or CPHD/DAS at the DAS concentration of 50 ng/mL. After 30 min of incubation, DiI-labeled fresh (non-activated) platelets were added. For platelet adhesion assay, the upper platelet suspension was dropped onto the surface of the glass slide. Free platelets were washed away with distilled water, and the platelets adhered to the slide surface were imaged under confocal laser scanning microscope (CLSM) (TCS-SP8 SR, Leica Microsystems, Wetzlar, Germany). For platelet aggregation assay, the upper free platelets were washed with PBS and the platelet aggregates formed in confocal dishes were then observed under CLSM.

2.9. *In vitro regulation efficiency of PSCs*

PSCs seeded in 96-well plates were co-incubated with different formulations diluted by culture medium containing 1% FBS and 10 ng/mL of TGF-β for 48 h. Then, 20 μL of MTT was added to each well and incubated for another 4 h. After removing the culture medium, 150 μL of DMSO was added to dissolve the formazan crystals. The absorbance was measured by a microplate spectrophotometer at 570 nm. The untreated activated PSCs were used as the control group, and the blank well was the blank group. The cell viability was calculated according to Eq. (6):

$$\text{Cell viability}\ (\%) = \left(\text{Absorbance}_{\text{samples}} - \text{Absorbance}_{\text{blank}}\right) \Big/ \left(\text{Absorbance}_{\text{control}} - \text{Absorbance}_{\text{blank}}\right) \times 100 \quad (6)$$

The TGF-β pretreated PSCs were seeded in 6-well plates and incubated with free DAS, PHD/DAS or CPHD/DAS (1 μg/mL of DAS) for 8 h. Besides, two cell groups were pre-incubated with 25 mmol/L HA for 2 h, followed by exposure to PHD/DAS or CPHD/DAS for 8 h. Then, the cells were lysed. The DAS concentration in the lysate was detected by HPLC. The cellular protein amount was quantified using a BCA protein assay kit. The cellular uptake efficiency was calculated according to Eq. (7):

$$\text{Uptake of DAS}\ (\mu\text{g}/\text{mg}) = Q_{DAS} \Big/ Q_{protein} \quad (7)$$

where Q_{DAS} is the DAS amount in lysate and Q_{protein} is the cellular protein amount.

PSCs were seeded into confocal dishes and co-treated with DAS, PHD/DAS or CPHD/DAS (2.5 μg/mL of DAS) and 10 ng/mL of TGF-β for 48 h. After being washed with PBS, the PSCs were incubated with 10 μmol/L Nile red in the dark for 30 min. Lipid droplets were observed by an inverted fluorescence microscope (Olympus IX53, Olympus Corporation, Tokyo, Japan). Besides, the PBS-washed cells were fixed in 4% paraformaldehyde for 15 min and then permeated in Triton X-100 for 10 min. After being sealed with 1% BSA for 30 min, the cells were incubated with α-SMA primary antibody (1:500) or fibronectin primary antibody (1:500) at 4 °C overnight, followed by incubation with anti-rabbit IgG Alexa Fluor 488 secondary antibody (1:500) for 1 h at room temperature. Finally, the cells were stained with Hoechst 33342 (10 μg/mL) for 15 min and observed by CLSM.

PSCs were seeded in 6-well plates and treated as described above. The culture medium was collected, and 60 μL of RIPA lysis buffer supplemented with 1 mmol/L phenylmethanesulfonyl fluoride and phosphatase inhibitor was added into the well. After the cells were fully lysed, the supernatant was collected. The culture medium and supernatant were mixed to obtain the total protein extract. The total protein content of the extract was detected by the BCA protein assay kit. Phospho-SRC, collagen I, α-SMA and fibronectin were then analyzed by Western blot (WB) technology.

2.10. *In vitro inhibition efficiency on Panc02*

The *in vitro* cytotoxicity of CPHD, PHD, free DAS, PHD/DAS and CPHD/DAS was evaluated by MTT assay. Panc02 cells seeded in 96-well plates were incubated with different formulations diluted at a series of concentrations for 48 h. Then, 20 μL of MTT was added to each well and incubated for another 4 h. After removing the medium, 150 μL of DMSO was added to dissolve the formazan crystals. The absorbance was measured by a microplate spectrophotometer at 570 nm. The untreated Panc02 was used as the control group, and the blank well was the blank group. The cell viability was calculated according to Eq. (8):

$$\text{Cell viability}\ (\%) = \left(\text{Absorbance}_{\text{samples}} - \text{Absorbance}_{\text{blank}}\right) \Big/ \left(\text{Absorbance}_{\text{control}} - \text{Absorbance}_{\text{blank}}\right) \times 100 \quad (8)$$

The uptake efficiency of Panc02 was characterized as described in Section 2.9. The apoptosis-inducing capability of DAS, PHD/DAS and CPHD/DAS was further evaluated by flow cytometry. Panc02 cells seeded in 12-well plates were treated with formulations diluted by medium at the DAS concentration of 50 ng/mL for 48 h. Then, the cells were processed using Annexin V-FITC/PI apoptosis detection kit according to procedures of the manufacturer. The samples were analyzed using flow cytometry (FACSCelesta, Becton, Dickinson and Company, Franklin Lakes, NJ, USA).

2.11. *In vivo distribution and tumor targeting*

Cy7 was co-encapsulated into micelles to obtain PHD/(DAS&Cy7) and CPHD/(DAS&Cy7). The PHD/(DAS&Cy7) and CPHD/(DAS&Cy7) were prepared as described in Section 2.5, apart from the change of "5 mg of DAS dissolved in 50 μL of DMF" to "5 mg of DAS and 0.5 mg Cy7 dissolved in 50 μL of DMF". C57BL/6 mice were *in situ* inoculated with Panc02-Luc cells. After 14 days, CPHD/(DAS&Cy7), PHD/(DAS&Cy7) or DAS&Cy7 was intravenously injected into the mice at a dose of 0.5 mg/kg Cy7. The mice were anesthetized and imaged by an *in vivo* Imaging Systems spectrum imaging system (PerkinElmer, Waltham, MA, USA) at 12, 20 and 36 h after administration. The mice were sacrificed, and the heart, liver, spleen, lung, kidney and tumor tissues were excised for *ex vivo* imaging at 36 h post-treatment. The data analysis was performed by the instrument software. The content of DAS in the tissues was quantified by HPLC after tissue homogenization. The tumors excised were frozenly sectioned at a thickness of 10 μm. The tumor slices were stained with CD31 and fibrin antibody, and observed using CLSM. In addition, to further evaluate the role of CREKA in CPHD/DAS targeting, after pre-administration of CREKA (5 mg/kg) for 2 h, CPHD/(DAS&Cy7) was intravenously injected. The tumor was harvested at 12 h post-injection, subjected to CD31 and fibrin staining, and imaged by CLSM.

2.12. *In vivo remodeling of tumor microenvironment*

The CPHD/Ticagrelor (Tic) was prepared as described in Section 2.5, with the change of "5 mg of DAS dissolved in 50 μL of DMF" to "5 mg of Tic dissolved in 50 μL of DMF". C57BL/6 mice were *in situ* inoculated with Panc02-Luc cells. After 14 days, mice were divided into three groups and i.v. injected with CPHD/DAS, CPHD/Tic or saline every other day for six injections at the dose of 5 mg/kg DAS or Tic (the time of first administration was recorded as Day 1). At the predetermined time, CPHD/(DAS&Cy7) was i.v. injected. The tumors were excised at 12 h post-injection, stained for CD31 and fibrin, and imaged with CLSM. To visualize the alteration of tumor functional vasculatures, FITC-lectin was injected into the representative mice on the designated days, and the mice were sacrificed 10 min later. The tumor tissues were frozenly sectioned. Endothelial cells were stained with anti-CD31 antibody and nuclei were stained with DAPI. CLSM was used to photograph, and lectin$^+$CD31$^+$/CD31$^+$ regions ($n = 3$) were calculated. The FITC-lectin and CD31 co-staining method is widely accepted for functional vessel identification[1,6,20]. In addition, CD31 single chromogenic sections were conducted and photographed with CLSM to observe the integrity and continuity changes of tumor vessels during the treatment. Besides, the tumor H&E staining was performed to investigate the progress of erythrocyte extravasation area and cell density. Immunofluorescence (IF) staining of α-SMA and Masson staining were prepared to inspect the tumoral alteration of activated PSCs and matrix. IFP measurements were performed *in vivo* with the

wick-in-needle technique prior to tumor excision, according to established protocols[44]. On Days 0, 12 of saline group and Days 4, 8, 12 of CPHD/DAS group, CPHD/(DAS&Cou6) obtained by mixing fluorescence probe Coumarin 6 (Cou6) with DAS during fabrication was injected into the mice. The tumors were removed 12 h later. Then, the nuclear chromogenic tumor sections were made for full section scanning to observe the tumoral penetration of Cou6. Meanwhile, tumoral Cou6 content was quantified by a microplate reader after tissue homogenization.

2.13. *In vivo antitumor efficacy*

C57BL/6 mice were *in situ* inoculated with Panc02-Luc cells, and the time of inoculation was recorded as Day 1. After two weeks, mice were randomly divided into 4 groups ($n = 11$). Mice were i.v. injected with CPHD/DAS, PHD/DAS, free DAS or saline every other day for 6 injections at a dose of 5 mg/kg (DAS). The orthotopic tumor was monitored by bioluminescent imaging at Days 14, 17, 20, 23 and 26. For bioluminescence imaging, D-luciferin potassium salt (150 mg/kg) was intraperitoneally injected and the mice were imaged using an AniView100 *in vivo* imaging system (Biolight Biotechnology Co., Ltd., Guangzhou, China) after 10 min. The body weights of mice were recorded every other day. On Day 28, mice were sacrificed and the tumors were harvested, weighed and pictured. The metastatic sites on critical tissues were counted and pictured. For WB analysis, tumors were homogenized on ice in RIPA lysis buffer containing phenylmethanesulfonyl fluoride and phosphatase inhibitor. The supernatants were collected for the phospho-SRC analysis. The excised tumors were fixed and sectioned for further study. H&E staining was conducted to investigate tumoral necrosis and hemorrhage, while TUNEL staining was performed to inspect tumoral apoptosis. Immunohistochemical staining of CD41 was made to characterize the number of the activated tumor-associated platelets. IF staining of CD31 and scanning electron microscope (SEM) imaging of tumor vasculature were prepared to visualize the integrity and continuity of the tumor vascular wall. For SEM, mice were perfused with saline from the heart and the tumor tissues were then harvested, fixed with 2.5% glutaraldehyde, and dehydrated by successive incubation with 30%, 50%, 70%, 80%, 90%, and 100% ethanol. After critical-point drying, the samples were ion-sputtered and imaged with JEOL JSM-7900F SEM (JEOL Ltd., Tokyo, Japan). IF staining (α-SMA and Desmin) and Masson staining were used to explore the tumoral changes of activated PSCs and collagen. Six mice from each group were monitored for the survival analysis since the time of Panc02-Luc inoculation.

2.14. *In vivo safety evaluation*

After the treatment as described in Section 2.13, the tail tip of the mice was amputated and immersed in saline at 37 °C, and the tail bleeding time was recorded. Blood was harvested from retro-orbital venous plexus of the mouse for the whole blood analysis and the serum biochemistry test of alanine aminotransferase (ALT), aspartate aminotransferase (AST), urea nitrogen (BUN) and serum creatinine (Scr).

2.15. *Statistical analysis*

All the experiments were repeated at least three times unless otherwise mentioned and data are presented as mean ± standard deviation (SD). The statistical significance was tested by one-way analysis of variance (ANOVA) or two-tailed Student's *t*-test using GraphPad Prism. $^{*}P < 0.05$, $^{**}P < 0.01$ and $^{***}P < 0.001$ were considered significant, highly significant and extremely significant, respectively.

3. Results and discussion

3.1. *Synthesis and characterization of CPHD conjugates*

We synthesized CPHD according to the steps described in Fig. S1. The chemical structures of CPHD and its intermediate products (HA-DOCA, PHD) were characterized by ^{1}H NMR, FT-IR and elemental analysis. As shown in Fig. 1A, the characteristic peaks of DOCA, HA and PEG appeared at 0.5−1.6, 1.98 and 3.65 ppm, respectively. When CREKA was conjugated to the HA skeleton, the Mal characteristic peak at 6.86 ppm disappeared and the characteristic peak of CREKA appeared at 4.39 ppm. FT-IR spectra further supported the successful synthesis of CPHD. As shown in Fig. 1B, the peaks at 3383 and 2873 cm^{-1} belonged to the $\nu_{(O-H)}$ and $\delta_{(C-H)}$ of HA. DOCA modification inducted the peaks at 1658 and 1538 cm^{-1} which were ascribed to the amide I band and amide II band. The strong peak at 1112 cm^{-1} corresponded to $\nu_{(C-O-C)}$ of PEG, indicating the successful conjugation of Mal-PEG3400-NH_2 to HA-DOCA. Since only CPHD contained S element, elemental analysis (Supporting Information Table S1) was then used to quantify the substitution ratio of CREKA peptide in CPHD. The corresponding result was 14.15% (*w*/*w*).

CPHD and PHD conjugates were dispersed in pure water to form micelles. As shown in Supporting Information Table S2, the hydrated sizes of the micelles were approximately 180 nm with uniform distribution (PDI <0.25), while their Zeta potentials were negative and close to each other (∼−13 mV). Then, the CMC of CPHD and PHD were determined as 90.84 and 75.91 mg/L, respectively (Supporting Information Fig. S2). The CMC values of the both conjugates significantly surpassed those of certain small molecular surfactants, suggesting their resistance against physiological dilution and potential capability of blood transport.

3.2. *Preparation and characterization of drug-loaded nano-micelles*

The particle size, PDI, Zeta potential, EE and DL rate of drug-loaded nano-micelles (PHD/DAS and CPHD/DAS) were shown in Supporting Information Table S3. Because of the hydrophobic interaction between drug carriers and DAS to form compact micelles, the particle sizes of CPHD/DAS and PHD/DAS decreased to around 80 nm. Meanwhile, their PDI and Zeta potential were similar to those of the blank micelles. Moreover, CPHD/DAS and PHD/DAS reached a high DL rate of 17.2% and 20.8%, suggesting their excellent drug-loading performance. The near spherical morphology and size (∼80 nm) of PHD/DAS and CPHD/DAS were shown in Fig. 1C and D.

Structural disintegration would lead to size change and drug leakage. FRET technique is a common approach for evaluating the blood stability of nanoparticles. The changes of FRET ratio reflect molecular distance alterations between FRET pair. This serves as an indicator of nanoparticle integrity[20,29]. As shown in Supporting Information Figs. S3 and S4, no remarkable size change of PHD/DAS or CPHD/DAS was observed in the simulated physiological

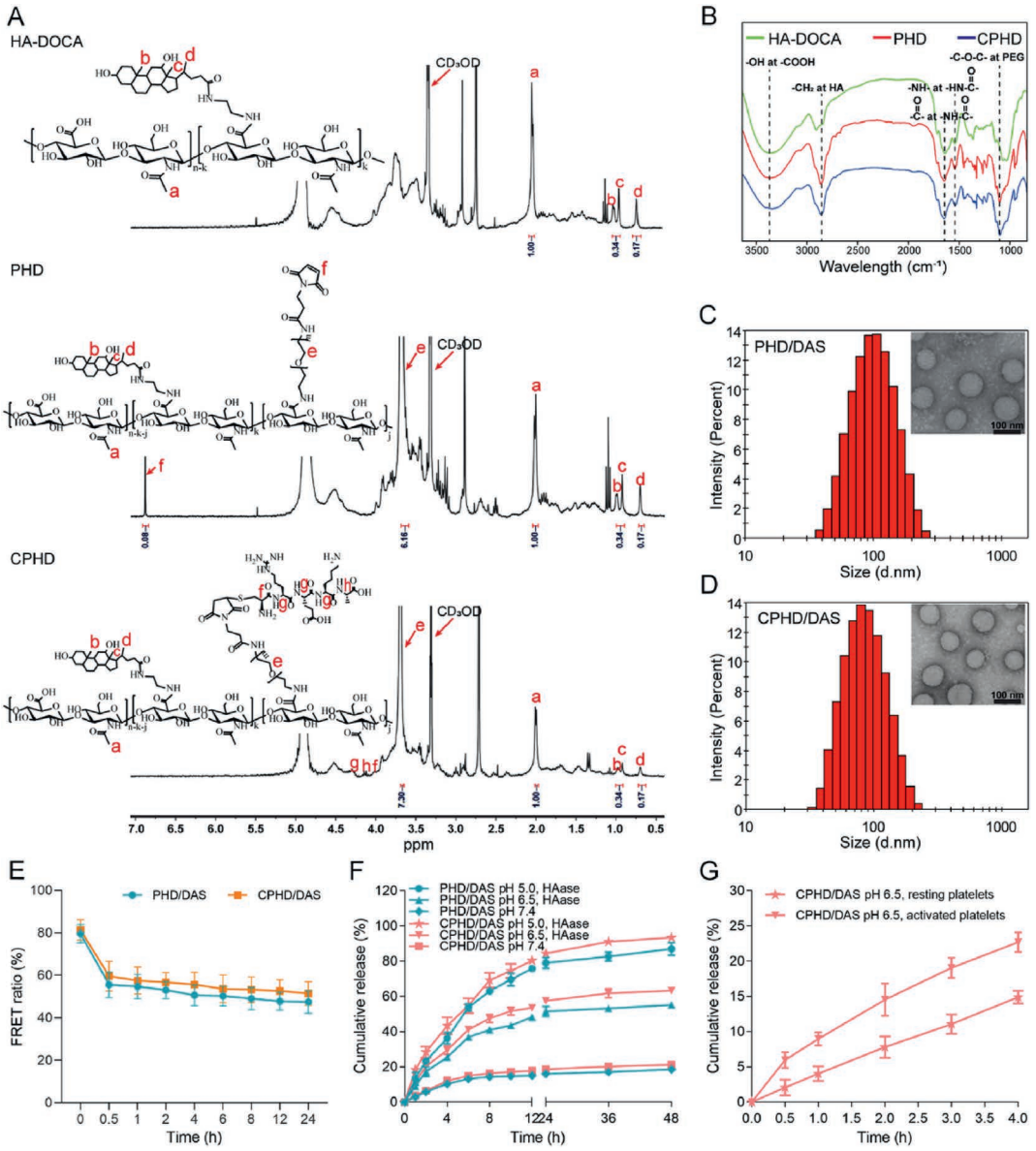

Figure 1 Characterizations of conjugates and drug-loaded nano-micelles. ^{1}H NMR spectra (A) and FT-IR spectra (B) of HA-DOCA, PHD and CPHD. Dynamic light scattering distribution and transmission electron microscopy image of PHD/DAS (C) and CPHD/DAS (D). (E) Fluorescence resonance energy transfer (FRET) ratios of DiO and DiI in PHD/DAS and CPHD/DAS at an excitation wavelength of 484 nm ($n = 3$). (F) pH and hyaluronidase (HAase) triggered DAS release from PHD/DAS and CPHD/DAS ($n = 3$). (G) Activated platelets triggered DAS release from CPHD/DAS ($n = 3$). Data are presented as mean ± SD.

conditions (PBS containing 10% FBS, culture medium) within 24 h. Besides, the FRET ratio in PHD/DAS and CPHD/DAS remained at approximately 50% at 24 h post-administration, demonstrating a certain degree in keeping micellar structure integrity (Fig. 1E). Furthermore, pharmacokinetic studies revealed rapid clearance of free DAS, whereas PHD/DAS and CPHD/DAS achieved prolonged systemic circulation (Supporting Information Fig. S5 and Table S4). This offered a potential promotion for further targeted accumulation.

Release behaviors of DAS from CPHD/DAS and PHD/DAS *in vitro* were studied by the dialysis method. pH 7.4 buffer was used as the release medium to simulate the blood environment. pH 6.5 or 5.0 buffer containing 0.5 mg/mL HAase was set to simulate PDAC microthrombi/matrix microenvironment and endosomal/lysosomal environment, respectively. Moreover, to directly validate that HAase from the activated platelets triggered DAS release, nanodrugs were incubated with the activated platelets at pH 6.5. As shown in Fig. 1F and Supporting Information Fig. S6, CPHD/DAS and PHD/DAS were able to remain relatively stable at physiological pH and release DAS quickly in an acidic environment. Due to the acid-triggered protonation of the −NH− group, DAS experienced increased solubility (Supporting Information Fig. S7) and weakened interaction with the micellar hydrophobic cores. Additionally, HAase-sensitive DAS release behavior was depicted in the buffer containing HAase or the activated platelets (Fig. 1F and G). The membrane-expressed HAase from the activated platelets accelerated DAS release *via* HAase-mediated micelle degradation.

3.3. *In vitro function regulation of platelet*

Activated platelets contribute to vascular integrity by releasing soluble platelet factors for forming endothelial cell connections and microthrombi[8,45]. To evaluate the inhibition effect of CPHD/DAS on platelet activation, thrombin-activated platelets were first exposed to the preparations, then fresh platelets were added to assess their adhesion and aggregation behaviors on the non-physiological surfaces (Fig. 2A). As shown in Fig. 2B and C, all of the DAS-containing preparations inhibited adhesion and aggregation of the subsequently added platelets, indicating suppressed activation. Owing to HAase (from activated platelets) triggered DAS release, micellar encapsulation did not affect the inhibitory effect of DAS on platelet activation[46].

3.4. *In vitro function regulation of PSCs*

Abnormally activated PSCs, a major role in the development of desmoplastic PDAC, exhibit excessive secretion of ECM components[3,47]. As shown in Fig. 2D, the conjugates had no notable cytotoxicity on PSCs in a wide concentration range (0.1−1000 μg/mL), indicating their favorable biosafety. Generally, the activated PSCs proliferate faster[48]. The cell proliferation of TGF-β co-treated PSCs was inhibited following the treatment of DAS-contained formulations (Fig. 2E), which was ascribed to the inhibition of PSCs activation *via* block of the downstream targets (SRC) of TGF-β signaling and platelet-derived growth factor receptor (Supporting Information Fig. S8). Resting PSCs are rich in lipid droplets, while activated PSCs lose lipid droplets storage and exhibit high expression of α-SMA, fibronectin and collagen I[2,20]. Thus, to evaluate the effect of DAS preparations on PSCs activation, fluorescence staining was used to visualize lipid droplet content, while IF staining and WB experiments were used to investigate the expression changes of characteristic proteins. As shown in Fig. 2F−I, all of the treated groups presented up-regulated lipid droplet content and down-regulated α-SMA, fibronectin and collagen I. Owing to enhanced cellular internalization (Supporting Information Fig. S9), CPHD/DAS

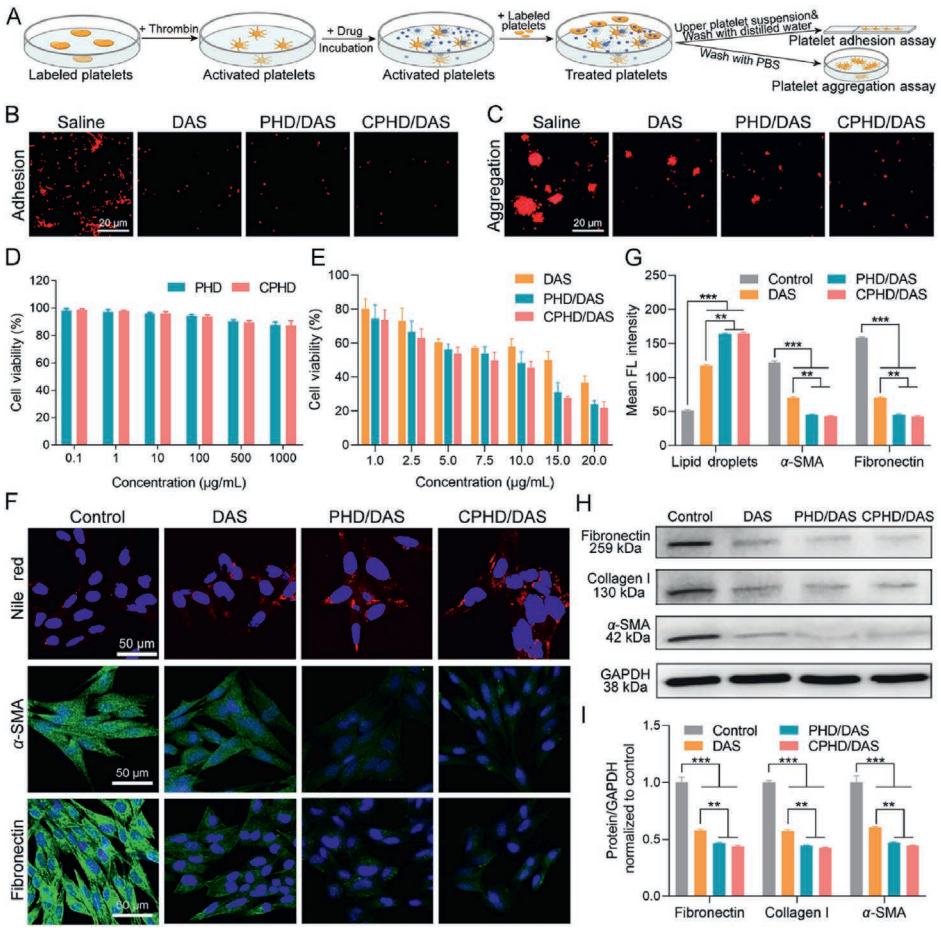

Figure 2 Inhibition of platelet activation and PSCs activation by CPHD/DAS. (A) Schematic illustration of the platelet adhesion and aggregation test experimental procedure. Effects of DAS, PHD/DAS or CPHD/DAS on platelet adhesion (B) and aggregation (C). (D) The viability of PSCs after incubation with conjugates and TGF-β for 48 h (n = 6). (E) The viability of PSCs after incubation with various preparations at different DAS concentrations and TGF-β for 48 h (n = 6). (F) Nile red staining of lipid droplets, immunofluorescence (IF) staining of α-SMA and fibronectin in PSCs after treatment with the indicated formulations and TGF-β for 48 h. (G) The mean fluorescence (FL) intensity of lipid droplets, α-SMA and fibronectin (n = 3). (H) WB analysis of PSCs markers after treatment with the indicated formulations and TGF-β for 48 h. (I) Quantitative analysis of data in WB assay using Image J normalized to the control group (n = 3). Data are presented as mean ± SD. Significance was tested using one-way ANOVA with Tukey's *post hoc* test. ***P < 0.001, **P < 0.01.

and PHD/DAS led to a more significant therapeutic effect than free DAS. These results evidenced that CPHD/DAS and PHD/DAS would remodel ECM homeostasis through PSCs regulation.

3.5. *In vivo distribution and tumor targeting*

In vivo imaging was conducted to determine whether CPHD/DAS could achieve tumor accumulation *via* CREKA-mediated microthrombi targeting. The systemic distribution of CPHD/(DAS&Cy7), PHD/(DAS&Cy7) and DAS&Cy7 at 12, 20, and 36 h after administration was observed. As exhibited, free DAS&Cy7 exhibited negligible tumor accumulation at 36 h post-injection, while CPHD/(DAS&Cy7) showed the strongest tumoral fluorescence signal (Fig. 3A and B). The *ex vivo* results further confirmed the superior tumor targeting ability of CPHD/(DAS&Cy7) and less accumulation in other organs (Fig. 3C and Supporting Information Fig. S10). Quantitative analysis of DAS mirrored imaging results (Fig. 3D). Then, CLSM revealed colocalization of CPHD/(DAS&Cy7) with fibrin in tumor microthrombi, which was nearly absent in free DAS&Cy7 and PHD/(DAS&Cy7) groups (Fig. 3E and Supporting Information Figs. S11−S14). Furthermore, we performed the competitive binding assay by pre-injecting free CREKA before administering CPHD/(DAS&Cy7), and the tumor accumulation was assessed. As exhibited in Supporting Information Fig. S15, CREKA pre-injection reduced tumor accumulation of CPHD/(DAS&Cy7), collectively confirming CREKA−fibrin interaction mediated tumor microthrombi targeting.

3.6. *In vivo regulation of tumor microenvironment*

Increased vascular leakage will increase the existing tumor IFP, which may seriously affect subsequent blood perfusion and convection of nanodrugs[11,49]. The reduction of solid stress in tumors can counteract the negative effect of IFP increase[5,50]. The *in vitro* results verified that CPHD/DAS successfully inhibited the activation of platelets and PSCs. Herein, it was speculated that CPHD/DAS tended to synchronously increase vascular leakage and reduce solid stress of the tumor, promoting continuous up-regulation of functional tumor vessels during the treatment.

To investigate whether CPHD/DAS could continuously augment functional vasculature proportion and tumoral drug accumulation during consecutive administration, the TME regulation experiments were conducted on the orthotopic Panc02 model. First, CPHD/DAS progressively increased endothelial gaps as time extended, leading to augmented erythrocyte extravasation and expanded bleeding area (Fig. 4A and B, Supporting Information Figs. S16 and S17). This result also indicated the exposure

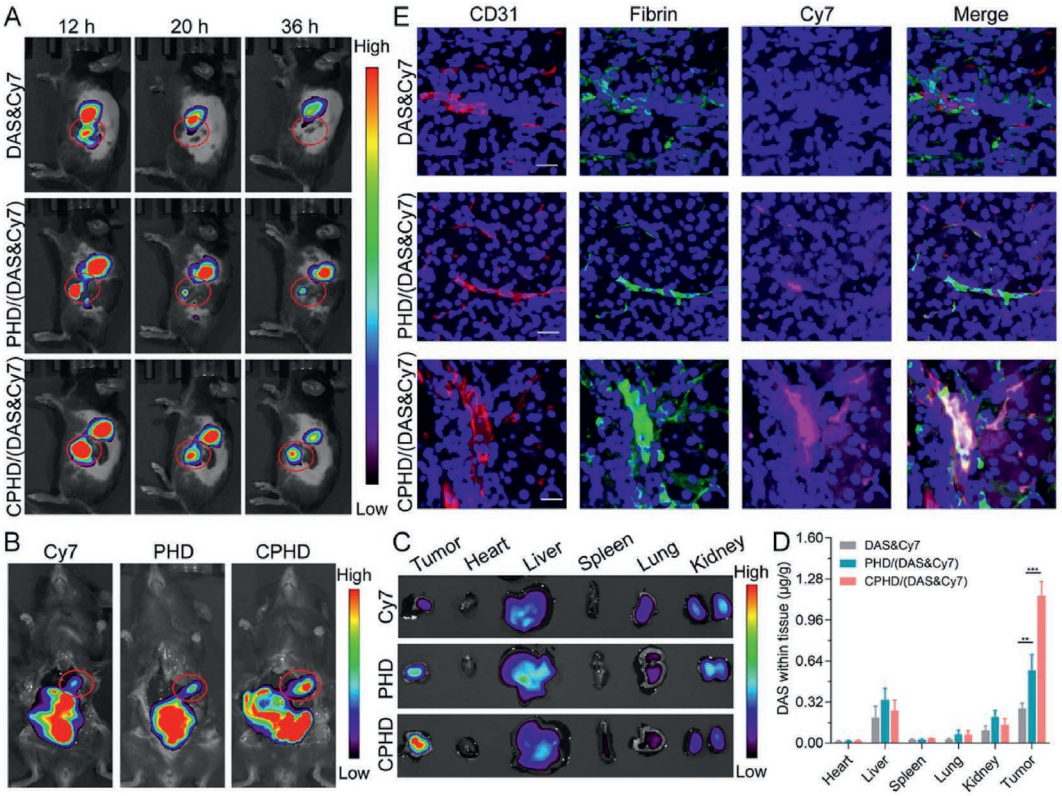

Figure 3 *In vivo* distribution and tumor targeting of different preparations. (A) *In vivo* imaging of orthotopic Panc02 tumor-bearing mice after intravenous injection of free DAS&Cy7, PHD/(DAS&Cy7), CPHD/(DAS&Cy7) at different time intervals. (B) *In vivo* fluorescence images of exposed abdominal tissues and (C) *Ex vivo* fluorescence images of tissues at 36 h after intravenous injection of DAS&Cy7 (abbreviated as Cy7), PHD/(DAS&Cy7) (abbreviated as PHD), and CPHD/(DAS&Cy7) (abbreviated as CPHD) into orthotopic Panc02 tumor-bearing mice. (D) Quantitative analysis of DAS content within different tissues. Data are presented as mean ± SD ($n = 3$). Significance was tested using one-way ANOVA with Tukey's *post hoc* test. ***$P < 0.001$, **$P < 0.01$. (E) CLSM images of frozen sections of tumors excised at 12 h post-injection of the above preparations. Blood vessels, fibrin and nuclei were stained with anti-CD31 (red) antibody, anti-fibrin (green) antibody and DAPI (blue), respectively. Scale bars represent 40 μm.

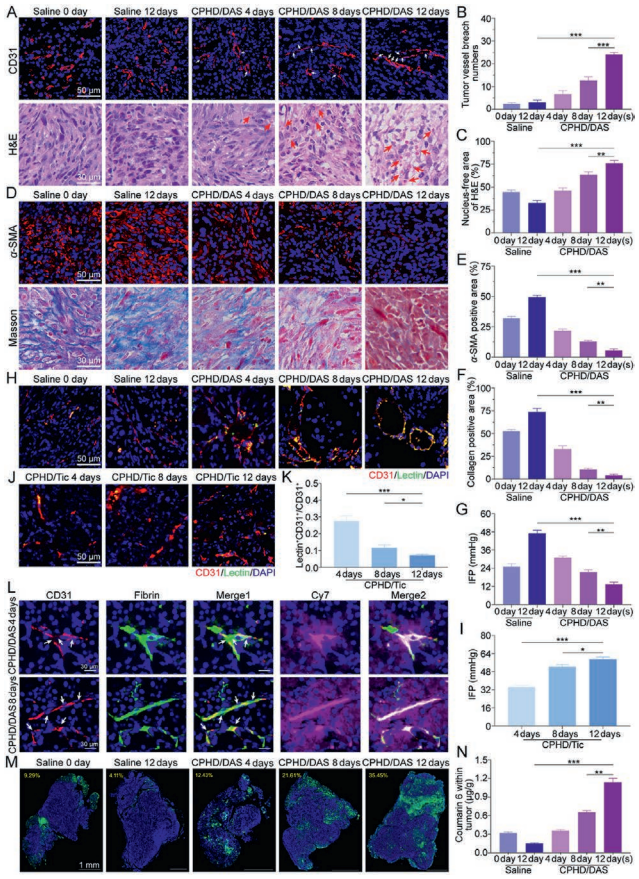

Figure 4 *In vivo* TME regulation of CPHD/DAS on tumor vasculature and matrix. (A) Characterization of tumor vascular permeability of saline and CPHD/DAS treated mice through IF staining of endothelial cells ($CD31^+$) and H&E staining. The white arrowheads indicated endothelial damage, while the red arrowheads indicated the bleeding area. The corresponding quantitative analysis of endothelial breaches (B) and nucleus-free area (C). (D) IF staining of α-SMA and Masson staining. The corresponding quantitative analysis of α-SMA (E) and collagen content (F). Interstitial fluid pressure (IFP) levels in tumors from saline and CPHD/DAS treated mice (G), CPHD/Tic treated mice (I) at the preset days. Fluorescence images of functional perfused vessels ($CD31^+$ $Lectin^+$) and total vessels ($CD31^+$) in tumors from saline and CPHD/DAS treated mice (H), CPHD/Tic treated mice (J) at the preset days. (K) The corresponding quantitative analysis of the ratio of functional vessels to total vessels. The quantification in B, C, E, F and K was based on three randomly selected microscopic fields by Image J. (L) CLSM images of frozen sections of tumors excised at 12 h post-injection of CPHD/(DAS&Cy7). The white arrowheads indicated endothelial damage. Fluorescence images of Cou6 (M) and quantitative analysis of Cou6 content (N) within the whole tumors harvested at 12 h post CPHD/(DAS&Cou6) injection. Data are presented as mean ± SD ($n = 3$). Significance was tested using one-way ANOVA with Tukey's *post hoc* test. *$P < 0.05$, **$P < 0.01$, ***$P < 0.001$.

of sub-vascular matrix. Meanwhile, α-SMA IF staining and Masson staining results showed a continuous decrease in the amounts of activated PSCs and collagen during CPHD/DAS treatments (Fig. 4D−F, Supporting Information Figs. S18 and S19). The ECM remodeling progressively counterbalanced the contribution of enhanced vascular permeability in elevating IFP (Fig. 4G). Then, the synchronized endothelial gap opening and matrix decompression resulted in a sustained increase in the proportion of functional vessels ($CD31^+$ $Lectin^+$) and blood perfusion (Fig. 4H, Supporting Information Figs. S20 and S21). Tic, a platelet activation inhibitor, was encapsulated into CPHD to investigate the effect of simple endothelial gap opening on tumor vascular function. CPHD/Tic could only increase vascular leakage. Consequently, tumor IFP gradually elevated (Fig. 4I) owing to the increased fluid extravasation and inherently dense ECM. The elevated IFP caused a progressive reduction in functional vasculature throughout CPHD/Tic treatment (Fig. 4J and K). Finally, we visualized and quantified the tumoral drug delivery efficiency after TME regulation by injecting the DAS/fluorescence probe co-loaded micelle CPHD/(DAS&Cy7) or CPHD/(DAS&Cou6) into the treated mice at the preset days. As shown in Fig. 4L and Supporting Information Figs. S22 and S23, CPHD/DAS treatment increased endothelial gaps and sub-vascular matrix exposure, which formed positive feedback-based self-propelling of tumoral accumulation with the CREKA-mediated targeting. Resultantly, the distribution and tumoral content of Cou6 continuously expanded through the whole tumor section during CPHD/DAS treatment (Fig. 4M and N). The achieved efficient drug delivery contributed to the final appreciably decreased tumoral cell density (Fig. 4C). In summary, the microthrombi targeted CPHD/DAS could synchronize endothelial gap opening and matrix decompression for a sustained augmentation of drug perfusion and penetration within PDAC.

3.7. *In vitro and in vivo antitumor potency*

MTT assay was used to detect the cytotoxicity of blank and drug-loaded micelles on Panc02 cells. As shown in Fig. 5A, the conjugates had no significant cytotoxicity on Panc02 cells within the concentration range of 0.1−1000 μg/mL. CPHD/DAS and PHD/DAS exhibited comparable cytotoxicity on Panc02 cells. Their IC_{50} values (∼55 ng/mL) were lower ($P < 0.05$) than that of free DAS (71.02 ng/mL) (Fig. 5B and Supporting Information Table S5). This was attributed to HA-mediated efficient internalization of drug-loaded micelles into Panc02 cells (Supporting Information Fig. S24). The *in vitro* antitumor ability of drug-loaded micelles was also validated by Annexin V-FITC/PI cell apoptosis assay. DAS-containing groups induced early and late apoptosis of Panc02 cells (Supporting Information Fig. S25). The total apoptosis rates induced by CPHD/DAS and PHD/DAS were higher than those induced by free DAS (Fig. 5C). These results further demonstrated the potential of the nano-micelles for PDAC treatment.

The *in vivo* antitumor effect of CPHD/DAS was further evaluated in the orthotopic PDAC mouse model. Bioluminescence imaging was used to monitor tumor growth (Fig. 5D and E). All of the DAS-contained groups exhibited tumor growth inhibition potency (Supporting Information Figs. S26 and S27). The self-propelled CPHD/DAS achieved the optimal tumor suppression with an inhibition rate of 70.72%, higher than that of PHD/DAS (53.01%) and free DAS (34.72%). The activity of SRC in tumors was evaluated by WB. As shown in Supporting Information Fig. S28, CPHD/DAS achieved superior SRC inhibition efficacy compared to PHD/DAS and free DAS, correlating with its enhanced tumor infiltration. Benefited from the efficient tumor-killing and the intrinsic anti-metastatic activity of DAS based on SRC kinases inhibition, CPHD/DAS also outperformed the other groups in metastasis inhibition of PDAC (Supporting Information Figs. S29 and S30, Fig. 5F). Consistent with the previous results,

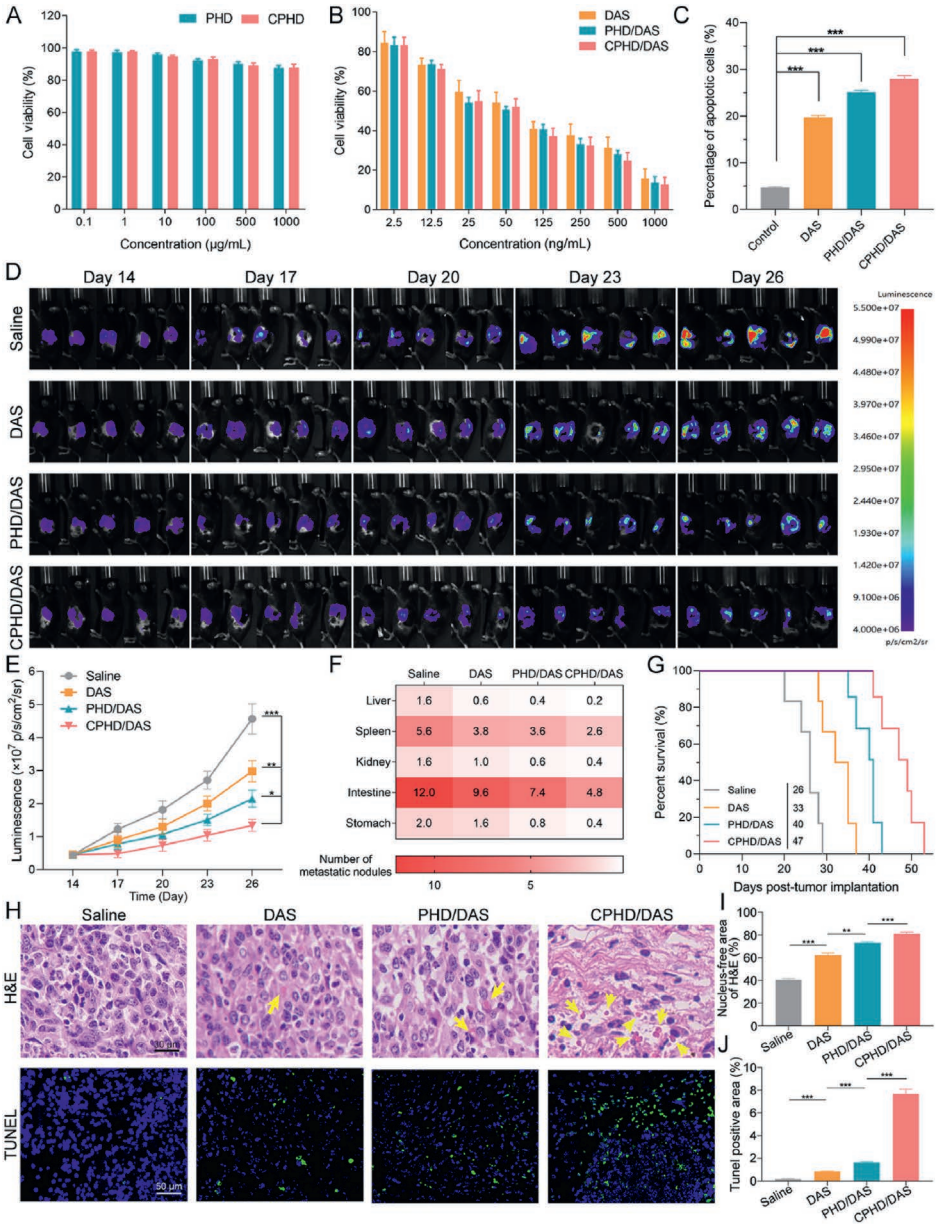

Figure 5 *In vitro* and *in vivo* antitumor efficiency of formulations in the PDAC model. (A) The viability of Panc02 cells after incubation with PHD or CPHD for 48 h ($n = 6$). (B) The viability of Panc02 cells after incubation with various preparations at different DAS concentrations for 48 h ($n = 6$). (C) The apoptosis quantitative analysis of Panc02 induced by different preparations for 48 h ($n = 3$). (D) *In vivo* bioluminescence images of mice treated with different formulations on Days 14, 17, 20, 23 and 26 ($n = 5$). (E) Tumor growth curves figured by the *in vivo* bioluminescence signal quantifications ($n = 5$). (F) Heat map of tumor metastasis frequency in abdominal tissues from mice after the whole treatment ($n = 5$). (G) Survival graph and median survival time of orthotopic pancreatic tumor-bearing mice treated with different formulations ($n = 6$). (H) H&E and TUNEL staining images and the corresponding quantitative analysis (nucleus-free area, TUNEL-positive area) (I, J) of tumors from mice after the whole treatment. The yellow arrowheads indicated probable bleeding area. The quantification in I, J was based on three randomly selected microscopic fields by Image J. Data are presented as mean ± SD. Significance was tested using one-way ANOVA with Tukey's *post hoc* test. $^{*}P < 0.05$, $^{**}P < 0.01$, $^{***}P < 0.001$.

CPHD/DAS treatment displayed the longest medium survival time (47 days) of orthotopic PDAC mice (Fig. 5G), the maximum area (81.84%) of tumor remission in H&E staining assay and the highest apoptotic ratio in TUNEL staining assay (Fig. 5H–J, Supporting Information Fig. S31). CPHD/DAS demonstrated superior *in vivo* antitumor efficacy in orthotopic PDAC.

The physiological and pathological changes of the tumor after the whole treatment were further investigated to validate the lasting TME regulation based on synchronized endothelial gap opening and matrix decompression. We analyzed vascular permeability (SEM imaging, CD31 IF, H&E for erythrocyte extravasation), platelet activation (CD41 IHC), PSCs activation status (α-SMA IF, Desmin IF), and collagen deposition (Masson's trichrome). As depicted in Fig. 5H and Fig. S31, CPHD/DAS treatment increased erythrocyte extravasation within tumors. Additionally, CPHD/DAS suppressed platelet activation and achieved the highest increase in

vascular permeability among all groups, which was beneficial for drug extravasation (Fig. 6A−D, Supporting Information Fig. S32). α-SMA and Desmin are the biomarkers for activated PSCs and quiescent PSCs, respectively. Results in Fig. 6E−G exhibited that CPHD/DAS could exert the most intensive inhibition on PSCs activation, evidenced by the lowest α-SMA signal and highest Desmin signal. Consequently, it induced the least collagen secretion (Fig. 6E and H). Histological analysis confirmed CPHD/DAS achieved lasting TME remodeling *in vivo*.

3.8. *In vitro and in vivo safety evaluation*

The *in vitro* and *in vivo* biosafety of the conjugates and drug-containing preparations was finally investigated. When the conjugate concentration was less than 6 mg/mL and the DAS concentration was less than 1 mg/mL, the corresponding hemolysis was less than 4% (Supporting Information Fig. S33), meeting the general hemolysis limit of 5%. During *in vivo* antitumor evaluation, all the treated mice did not show a significant change in body weight or in liver/kidney toxicity index (ALT, AST, Bun and Scr) (Supporting Information Figs. S34A and S35A). Because of the nonspecific biodistribution affecting the circulating platelets, free DAS-treated mice exhibited a prolonged bleeding time after the tail cut (Fig. S34B). Besides, all of the blood routine indicators from free DAS-treated mice fell outside the normal range (Fig. S35B). In contrast, the active-targeted and self-propelled tumor drug delivery endowed by CPHD/DAS reduced the systemic toxicity of DAS. CPHD/DAS

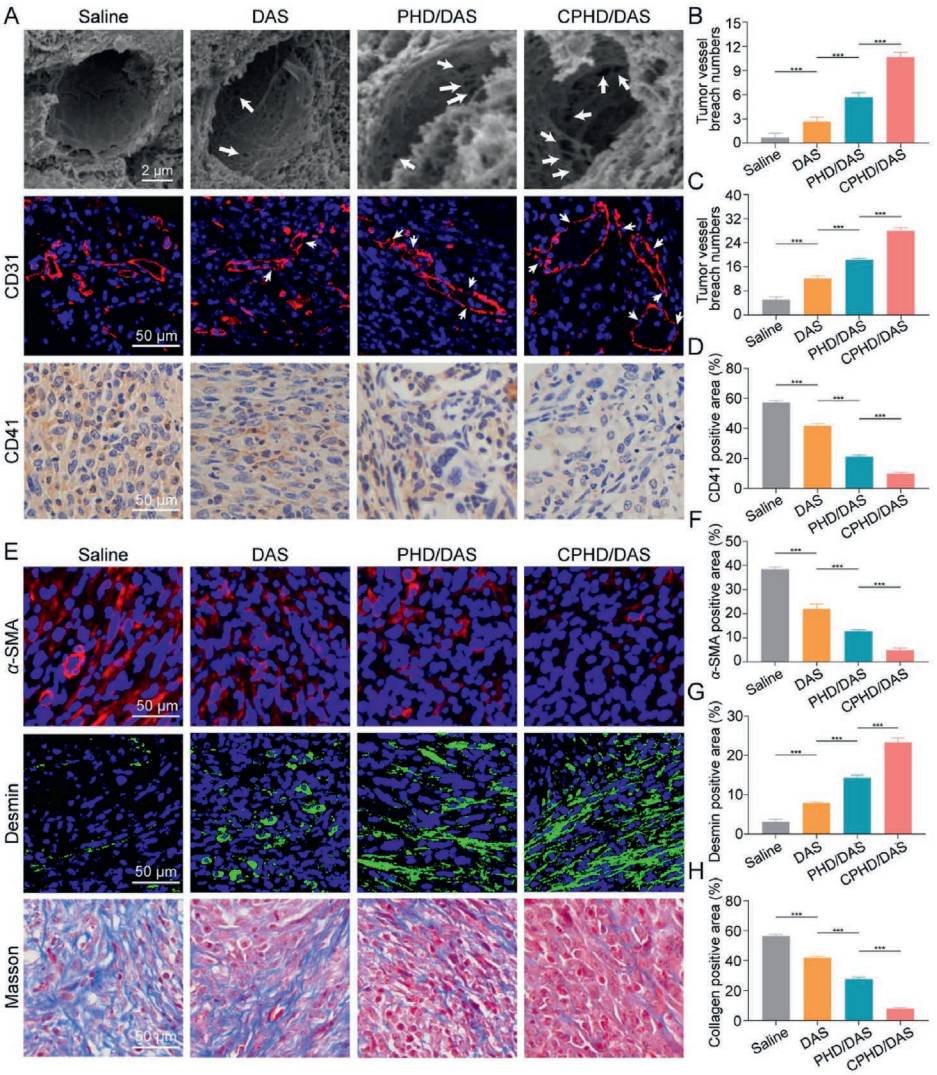

Figure 6 Histopathological examination of tumors harvested from mice after the whole treatment with different formulations. Scanning electron microscope image of tumor vasculature (A) and quantitative analysis of endothelial breaches (B). The white arrowheads indicated endothelial gaps. IF staining with CD31 antibody for endothelial cells (A) and quantitative analysis of endothelial breaches (C). The white arrowheads indicated endothelial damage. Immunohistochemical staining with CD41 antibody for activated platelets (A) and quantitative analysis of CD41 positive area (D). IF staining of α-SMA and Desmin in tumor PSCs (E) and quantitative analysis of α-SMA positive area (F), Desmin positive area (G). Masson staining for collagen within tumor (E) and quantitative analysis of collagen-positive area (H). The quantification in B−D and F−H was based on three randomly selected microscopic fields by Image J. Data are presented as mean ± SD. Significance was tested using one-way ANOVA with Tukey's *post hoc* test. ***$P < 0.001$.

demonstrated a potent antitumor potency with satisfactory biosafety.

4. Conclusions

We fabricated the tumor microthrombi/matrix-targeted nanodrug (CPHD/DAS) which integrated fibrin targeted-HAase responsive conjugates and a multi-target tyrosine kinase inhibitor for endothelial gap opening and matrix decompression. CPHD/DAS could concentrate DAS around tumor vascular walls, thus increasing vascular leakage and matrix exposure *via* platelets activation inhibition. The matrix exposure formed positive feedback-based self-propelling in drug accumulation with the CREKA-mediated targeting. The accumulated DAS suppressed PSCs activation for matrix decompression. Finally, the reduced tumoral solid stress gradually counterbalanced the contribution of enhanced vascular permeability in elevating IFP, realizing sustained augmentation of functional tumor vessels during the treatment. Consequently, efficient tumoral drug infiltration and antitumor efficacy were achieved in Panc02 tumor. Based on the comprehensive consideration of TME affecting drug perfusion, our strategy provides a new case to improve the efficiency and expand the application scope of the "EPR amplification" strategy in antitumor therapy. It also offers new insights for PDAC treatment.

Acknowledgments

This study was supported by the project of the National Natural Science Foundation of China (Nos. 81972835 and 81703442), Qing Lan Project of Jiangsu Province (China).

Author contributions

Mengnan Yang: Writing - review & editing, Data curation, Investigation, Methodology, Writing - original draft. Yuqing Tong: Writing - original draft, Formal analysis, Investigation, Writing - review & editing. Shaoping Yin: Methodology, Investigation, Writing - original draft. Hengchuan Zhang: Validation, Writing - review & editing. Xiaowen Huang: Writing - review & editing, Data curation. Kai Yuan: Writing - review & editing. Yanfei Hao: Methodology. Jianping Zhou: Funding acquisition, Project administration. Meirong Huo: Funding acquisition, Project administration. Tingjie Yin: Funding acquisition, Project administration, Data curation, Formal analysis.

Conflicts of interest

The authors declare no conflicts of interest.

Appendix A. Supporting information

Supporting information to this article can be found online at https://doi.org/10.1016/j.apsb.2025.12.037.

References

1. Wu ZQ, Wu Y, Wang MM, Chen DG, Lv JJ, Yan J, et al. FAP-activated liposomes achieved specific macropinocytosis uptake by pancreatic stellate cells for efficient desmoplasia reversal. *Chem Eng J* 2024;**495**:153369.
2. Duan NX, Li JJ, Song S, Wang F, Yang YW, Nie D, et al. Enzyme-activated prodrug-based smart liposomes specifically enhance tumor hemoperfusion with efficient drug delivery to pancreatic cancer cells and stellate cells. *Adv Funct Mater* 2021;**31**:2100605.
3. Chen XH, Jia F, Li YZ, Deng YY, Huang Y, Liu WF, et al. Nitric oxide-induced stromal depletion for improved nanoparticle penetration in pancreatic cancer treatment. *Biomaterials* 2020;**246**:119999.
4. Zhang B, Jiang T, Shen S, She XJ, Tuo YY, Hu Y, et al. Cyclopamine disrupts tumor extracellular matrix and improves the distribution and efficacy of nanotherapeutics in pancreatic cancer. *Biomaterials* 2016; **103**:12−21.
5. Mei T, Shashni B, Maeda H, Nagasaki Y. Fibrinolytic tissue plasminogen activator installed redox-active nanoparticles (t-PA@iRNP) for cancer therapy. *Biomaterials* 2020;**259**:120290.
6. Wei Y, Song S, Duan NX, Wang F, Wang YX, Yang YW, et al. MT1-MMP-activated liposomes to improve tumor blood perfusion and drug delivery for enhanced pancreatic cancer therapy. *Adv Sci (Weinh)* 2020;**7**:1902746.
7. Setua S, Shabir S, Shaji P, Bulnes AM, Dhasmana A, Holla S, et al. Exosomes derived from tumor adjacent fibroblasts efficiently target pancreatic tumors. *Acta Pharm Sin B* 2024;**14**:3009−26.
8. Ho-Tin-Noé B, Boulaftali Y, Camerer E. Platelets and vascular integrity: how platelets prevent bleeding in inflammation. *Blood* 2018; **131**:277−88.
9. Ho-Tin-Noé B, Goerge T, Cifuni SM, Duerschmied D, Wagner DD. Platelet granule secretion continuously prevents intratumor hemorrhage. *Cancer Res* 2008;**68**:6851−8.
10. Han HJ, Hou Y, Chen XH, Zhang PS, Kang MX, Jin Q, et al. Metformin-induced stromal depletion to enhance the penetration of gemcitabine-loaded magnetic nanoparticles for pancreatic cancer targeted therapy. *J Am Chem Soc* 2020;**142**:4944−54.
11. Kirtane AR, Sadhukha T, Kim H, Khanna V, Koniar B, Panyam J. Fibrinolytic enzyme cotherapy improves tumor perfusion and therapeutic efficacy of anticancer nanomedicine. *Cancer Res* 2017;**77**: 1465−75.
12. Yu QW, Qiu Y, Li JP, Tang X, Wang XH, Cun XL, et al. Targeting cancer-associated fibroblasts by dual-responsive lipid-albumin nanoparticles to enhance drug perfusion for pancreatic tumor therapy. *J Control Release* 2020;**321**:564−75.
13. Zou LH, Xian P, Pu Q, Song YJ, Ni ST, Chen L, et al. Nano-drug delivery strategies affecting cancer-associated fibroblasts to reduce tumor metastasis. *Acta Pharm Sin B* 2025;**15**:1841−68.
14. Liu Y, Zhang YC, Li HK, Hu TY. Recent advances in the bench-to-bedside translation of cancer nanomedicines. *Acta Pharm Sin B* 2025;**15**:97−122.
15. Wang H, Qi L, Han H, Li XN, Han MM, Xing L, et al. Nanomedicine regulating PSC-mediated intercellular crosstalk: mechanisms and therapeutic strategies. *Acta Pharm Sin B* 2024;**14**:4756−75.
16. Ji TJ, Lang JY, Wang J, Cai R, Zhang YL, Qi FF, et al. Designing liposomes to suppress extracellular matrix expression to enhance drug penetration and pancreatic tumor therapy. *ACS Nano* 2017;**11**:8668−78.
17. Mardhian DF, Storm G, Bansal R, Prakash J. Nano-targeted relaxin impairs fibrosis and tumor growth in pancreatic cancer and improves the efficacy of gemcitabine *in vivo*. *J Control Release* 2018;**290**:1−10.
18. Li YK, Zhao Z, Liu H, Fetse JP, Jain A, Lin CY, et al. Development of a tumor-responsive nanopolyplex targeting pancreatic cancer cells and stroma. *ACS Appl Mater Interfaces* 2019;**11**:45390−403.
19. Han XX, Li YY, Xu Y, Zhao X, Zhang YL, Yang X, et al. Reversal of pancreatic desmoplasia by re-educating stellate cells with a tumour microenvironment-activated nanosystem. *Nat Commun* 2018;**9**:3390.
20. Cao JX, Wu J, Yang P, Qian K, Cheng YL, Xu MJ, et al. Dual enzyme cascade-activated popcorn-like nanoparticles efficiently remodeled stellate cells to alleviate pancreatic desmoplasia. *ACS Nano* 2023;**17**: 19793−809.
21. Cao JX, Yang P, Wang PZ, Xu ST, Cheng YL, Qian K, et al. "Adhesion and release" nanoparticle-mediated efficient inhibition of platelet activation disrupts endothelial barriers for enhanced drug delivery in tumors. *Biomaterials* 2021;**269**:120620.

22. Li SP, Zhang YL, Wang J, Zhao Y, Ji TJ, Zhao X, et al. Nanoparticle-mediated local depletion of tumour-associated platelets disrupts vascular barriers and augments drug accumulation in tumours. *Nat Biomed Eng* 2017;**1**:667−79.
23. Ma ZF, Liu S, Ke Y, Wang HZ, Chen RH, Xiang ZH, et al. Biomimetic nano-NOS mediated local NO release for inhibiting cancer-associated platelet activation and disrupting tumor vascular barriers. *Biomaterials* 2020;**255**:120141.
24. Zhou ZG, Zhang BL, Wang SS, Zai WJ, Yuan AH, Hu YQ, et al. Perfluorocarbon nanoparticles mediated platelet blocking disrupt vascular barriers to improve the efficacy of oxygen-sensitive antitumor drugs. *Small* 2018;**14**:e1801694.
25. Xiong W, Qi L, Si DL, Jiang X, Liu Y, Zheng CJ, et al. Effective tumor vessel barrier disruption mediated by perfluoro-*N*-(4-methylcyclohexyl) piperidine nanoparticles to enhance the efficacy of photodynamic therapy. *Nanoscale* 2021;**13**:13473−86.
26. Xu C, Yang S, Jiang ZJ, Zhou JP, Yao J. Self-propelled Gemini-like LMWH-scaffold nanodrugs for overall tumor microenvironment manipulation *via* macrophage reprogramming and vessel normalization. *Nano Lett* 2020;**20**:372−83.
27. Zhang B, Jiang T, She XJ, Shen S, Wang S, Deng J, et al. Fibrin degradation by rtPA enhances the delivery of nanotherapeutics to A549 tumors in nude mice. *Biomaterials* 2016;**96**:63−71.
28. Young A, Chapman O, Connor C, Poole C, Rose P, Kakkar AK. Thrombosis and cancer. *Nat Rev Clin Oncol* 2012;**9**:437−49.
29. Liu YH, Li LC, Liu JY, Yang MN, Wang HL, Chu XX, et al. Biomineralization-inspired dasatinib nanodrug with sequential infiltration for effective solid tumor treatment. *Biomaterials* 2021;**267**: 120481.
30. Zeng XL, Zhang YW, Xu X, Chen Z, Ma LL, Wang YS, et al. Construction of pH-sensitive targeted micelle system co-delivery with curcumin and dasatinib and evaluation of anti-liver cancer. *Drug Deliv* 2022;**29**:792−806.
31. Yao Q, Choi JH, Dai Z, Wang J, Kim D, Tang X, et al. Improving tumor specificity and anticancer activity of dasatinib by dual-targeted polymeric micelles. *ACS Appl Mater Interfaces* 2017;**9**: 36642−54.
32. Ye MJ, Hu JF, Han LL, Zhang HB, Xue P, Kang YJ, et al. Neighboring effect-initiated supramolecular nanocomplex with sequential infiltration as irreversible apoptosis inducer for synergetic chemo-immunotherapy. *Adv Sci (Weinh)* 2024;**11**:e2402809.
33. Zhang P, Li J, Ghazwani M, Zhao WC, Huang YX, Zhang XL, et al. Effective co-delivery of doxorubicin and dasatinib using a PEG-Fmoc nanocarrier for combination cancer chemotherapy. *Biomaterials* 2015; **67**:104−14.
34. Zhang X, Li XD, Sun SH, Wang P, Ma XT, Hou R, et al. Anti-tumor metastasis *via* platelet inhibitor combined with photothermal therapy under activatable fluorescence/magnetic resonance bimodal imaging guidance. *ACS Appl Mater Interfaces* 2021;**13**: 19679−94.
35. Gong ZR, Chen M, Ren QS, Yue XL, Dai ZF. Fibronectin-targeted dual-acting micelles for combination therapy of metastatic breast cancer. *Signal Transduct Targeted Ther* 2020;**5**:12.
36. Li R, Li YP, Zhang JH, Liu QH, Wu T, Zhou J, et al. Targeted delivery of celastrol to renal interstitial myofibroblasts using fibronectin-binding liposomes attenuates renal fibrosis and reduces systemic toxicity. *J Control Release* 2020;**320**:32−44.
37. Senis YA, Mazharian A, Mori J. Src family kinases: at the forefront of platelet activation. *Blood* 2014;**124**:2013−24.
38. Rayes J, Watson SP, Nieswandt B. Functional significance of the platelet immune receptors GPVI and CLEC-2. *J Clin Investig* 2019; **129**:12−23.
39. Cheng CJ, Liu KX, Zhang JL, Han YQ, Zhang TJ, Hou YY, et al. Ginsenoside CK targets PHD2 to prevent platelet adhesion and enhance blood circulation by modifying the three-dimensional arrangement of collagen. *Acta Pharm Sin B* 2025;**15**:1497−513.
40. Cao YH. Multifarious functions of PDGFs and PDGFRs in tumor growth and metastasis. *Trends Mol Med* 2013;**19**:460−73.
41. Roskoski R. Src protein—Tyrosine kinase structure, mechanism, and small molecule inhibitors. *Pharmacol Res* 2015;**94**:9−25.
42. Huo MR, Wang HL, Li LC, Tong YQ, Hu CX, Gu YW, et al. Redox-sensitive hyaluronic acid-cholesterol nanovehicles potentiate efficient transmembrane internalization and controlled release for penetrated "full-line" inhibition of pre-metastatic initiation. *J Control Release* 2021;**336**:89−104.
43. Brass LF. Thrombin and platelet activation. *Chest* 2003;**124**:18S−25S.
44. Martin JD, Panagi M, Wang CY, Khan TT, Martin MR, Voutouri C, et al. Dexamethasone increases cisplatin-loaded nanocarrier delivery and efficacy in metastatic breast cancer by normalizing the tumor microenvironment. *ACS Nano* 2019;**13**:6396−408.
45. Ye WL, Wang JJ, Little PJ, Zou JM, Zheng ZH, Lu J, et al. Anti-atherosclerotic effects and molecular targets of ginkgolide B from *Ginkgo biloba*. *Acta Pharm Sin B* 2024;**14**:1−19.
46. Albeiroti S, Ayasoufi K, Hill DR, Shen B, de la Motte CA. Platelet hyaluronidase-2: an enzyme that translocates to the surface upon activation to function in extracellular matrix degradation. *Blood* 2015; **125**:1460−9.
47. Chen XL, Zhou WX, Liang C, Shi S, Yu XJ, Chen QJ, et al. Co-delivery nanosystem targeting the deep microenvironment of pancreatic cancer. *Nano Lett* 2019;**19**:3527−34.
48. Huo MR, Zhou JY, Wang HL, Zheng YZ, Tong YQ, Zhou JP, et al. A pHe sensitive nanodrug for collaborative penetration and inhibition of metastatic tumors. *J Control Release* 2022;**352**:893−908.
49. Ho YJ, Chu SW, Liao EC, Fan CH, Chan HL, Wei KC, et al. Normalization of tumor vasculature by oxygen microbubbles with ultrasound. *Theranostics* 2019;**9**:7370−83.
50. Mpekris F, Papageorgis P, Polydorou C, Voutouri C, Kalli M, Pirentis AP, et al. Sonic-hedgehog pathway inhibition normalizes desmoplastic tumor microenvironment to improve chemo- and nanotherapy. *J Control Release* 2017;**261**:105−12.